Journal of Materials Chemistry C

ROYAL SOCIETY OF CHEMISTRY

PAPER

View Article Online
View Journal | View Issue

Cite this: J. Mater. Chem. C, 2022, 10, 13805

How to calibrate luminescent crossover thermometers: a note on "quasi"-Boltzmann systems†

Benedikt Bendel and Markus Suta *

Luminescent thermometers are potential material candidates for remote and non-invasive temperature sensing by means of a temperature-dependent optical signal. A particularly well-known class of luminescent thermometers are Boltzmann thermometers that rely on thermal coupling between two excited levels from the same configuration. Their thermal coupling kinetics is then governed by multiphonon transitions. A substantial part of potential luminescent thermometers does, however, rely on an interconfigurational crossover between two excited state potentials with differing equilibrium metal-ligand distances such as Cr^{3+} or Pr^{3+}. These thermometers are often characterized by much higher intrinsic non-radiative coupling rates that allow exploiting a much higher energy gap for high relative sensitivities at appreciably low temperatures. For this class of luminescent thermometers, fitting models are often merely effective and no clear guidelines on how to tune them or how to verify the physical reliability of the fit are available. In this work, we derive a generalized fitting model for luminescent crossover thermometers and demonstrate that they generally follow a "quasi"-Boltzmann law. We explicitly demonstrate the concepts on the established phosphor SrB_4O_7 : 0.5% Sm^{2+}. In this compound, Sm^{2+} can be efficiently excited with blue light and shows intense red $^5D_0 \rightarrow {}^7F_J$ (J = 0...6) luminescence above 680 nm and broad-banded $4f^55d^1 \rightarrow 4f^6$-related luminescence peaking at 585 nm. By additional time-resolved measurements, it is possible to independently assess the expected order of magnitude of the fitting parameters and thus, judge the physical content of the calibration model of a luminescent crossover thermometer. It is finally shown that crossover thermometers are characterized by high relative sensitivities and low-temperature measurement uncertainty at elevated temperatures but their liability toward thermal quenching poses a serious limitation to the dynamic working range of this class of thermometers.

Received 22nd March 2022,
Accepted 23rd April 2022

DOI: 10.1039/d2tc01152b

rsc.li/materials-c

1. Introduction

Luminescence thermometry has emerged as a promising alternative for non-invasive, remote temperature sensing and relies on the temperature dependence of the optical signals of luminescent compounds.[1–3] Its potential as a local non-invasive temperature probe has been shown in several niche applications ranging from catalysis[4,5] over biological processes[6] to heat transport phenomena at the micro-and nanoscale.[7–9]

Various readout options exist such as the intensity of a signal, the luminescence decay time, width, or position of an emission band. Among the different methodological concepts,[10–12] especially the ratiometric intensity approach exploiting the emission from two thermally coupled excited levels has become popular due to its simplicity and possibility for the fast readout (by the usage of sensitive CCD cameras for example). If the two emission bands of interest arise from two thermally coupled excited levels of the same configuration, the luminescence intensity ratio expectedly follows Boltzmann's law and can be linearized if plotted in the correct way.[13] This is particularly appealing for applications as linear calibration laws allow simple identification of systematic biases that are simple, and Boltzmann's law offers the possibility to readily verify the fitting parameter for its physical content.

Boltzmann-type thermalization between two excited levels and thus, the working concept of a ratiometric Boltzmann thermometer requires that the non-radiative transition rate responsible for the coupling of the two excited levels is larger than any radiative or non-radiative depopulation rate of the lower excited level.[13,14] Otherwise, the excited levels decouple,

Inorganic Photoactive Materials, Institute of Inorganic and Structural Chemistry, Heinrich Heine University Düsseldorf, Universitätsstraße 1, 40225 Düsseldorf, Germany. E-mail: markus.suta@hhu.de

† Electronic supplementary information (ESI) available: Powder X-ray diffraction pattern of synthesised SrB_4O_7:Sm^{2+} and temperature-dependent time-resolved luminescence measurements. See DOI: https://doi.org/10.1039/d2tc01152b

and thermometry with them is not possible anymore. Non-radiative transitions in crystalline solids rely on the thermal occupation of phonon modes and become faster with increasing temperature. However, the low-temperature onset for thermal coupling of the two excited levels depends on the ratio between the intrinsic non-radiative transition rate and radiative depopulation rate of the lower excited level. This ratio determines the dynamic working range of a luminescent Boltzmann thermometer.[13]

The lanthanoid ions with their rich spin–orbit energy-level structure arising from the $4f^n$ (n = 2–12) open-shell configuration are among the primary candidates for Boltzmann-based luminescence thermometry.[1] Their emission is characterized by high quenching temperatures and narrow linewidths due to the intraconfigurational character of the optical transitions, which offers an intrinsically high resolution of peaks from thermally coupled excited levels. Among the most significant limitations of Boltzmann thermometers are, however, their typically small non-radiative coupling rates that only allow use of energy gaps in the order of the thermal energies of interest ($\Delta E_{21} \sim k_B T$).

There are several luminescent thermometers that rely on thermalization between excited states with different equilibrium metal-ligand distances, which happens to enhance the non-radiative coupling strength between the thermalized states. One important class is dual-center energy transfer thermometers. Although very flexible, the temperature dependence of the luminescence intensity ratio is typically non-linear and requires more sophisticated (although physically still transparent!) modelling approaches.[15–18] Another related class with similar properties to the excited states are so-called ratiometric luminescent crossover thermometers. Examples include Cr^{3+} with its thermally coupled $^2E_{(g)}$ and $^4T_{2(g)}$ states in octahedral coordination,[19–21] or Pr^{3+}[22–24] with the excited $4f^15d^1$- and $4f^2(^3P_0)$-based emission. However, also organic emitters with so-called thermally activated delayed fluorescence based on thermally coupled singlet and triplet states have come into the focus of this potential application.[25–30] For these single-center luminescent thermometers, it is often simply assumed that the calibration of the luminescence intensity ratio from the thermally coupled emissions can be also fitted with Boltzmann's law. However, very often, deviations at low temperatures are observed, or physically non-meaningful fitting parameters are obtained. A critical re-evaluation of the foundations of the calibration model for this type of luminescent thermometer is, however, relevant for an appropriate judgement of their performance and reliability. Moreover, the derivation of a generalized, physically meaningful calibration model would help establish design principles or guidelines for luminescent crossover thermometers and how their properties could be tuned into a desirable range.

It was our goal within this work to establish a generalized model for luminescent crossover thermometers and experimental tests that on the representative example of SrB_4O_7: 0.5% Sm^{2+}. It is well-known that this tetraborate stabilizes several lanthanoid dopants in their divalent oxidation state even in the air. Sm^{2+} has a $4f^6$ configuration and can be efficiently excited with blue light into the $4f^55d^1$ configuration. This configuration is energetically close to the excited ^5D_J (J = 1, 2) spin–orbit levels,[31,32] in contrast to its isoelectronic trivalent analogue Eu^{3+}, in which the excited $4f^55d^1$ electronic configuration is located in the vacuum UV range.[33] This can be chemically intuitively understood by the much smaller absolute value of the reduction potential of Sm^{3+}/Sm^{2+} (E^0 = −1.55 V) compared to Eu^{4+}/Eu^{3+} (E^0 = +6.20 V).[34] The energetic proximity of the $4f^55d^1$ configuration and the radiatively emitting excited $^5D_0$ level offers the desired conditions for a configurational crossover and gives rise to a temperature-dependent change in the appearance of the luminescence spectra of Sm^{2+} in SrB_4O_7.[31,32] We show that our proposed generalized fitting model for luminescent crossover thermometers is physically reasonable, and the parameters can be related to independent time-resolved studies. Based on the calibration model, it is possible to evaluate the performance of the luminescent thermometer and compare it to that obtained on the conventional Boltzmann thermometers.

Markus Suta

Markus Suta (32) obtained his PhD degree in Chemistry in the group of Prof. Claudia Wickleder in 2017 and continued with a second degree in Physics (MSc) in the group of Prof. Thomas Mannel at the University of Siegen, Germany. He followed up with a postdoctoral stage in the group of Prof. Andries Meijerink at Utrecht University, Netherlands. Since May 2021, he has started an own research group as a tenure track assistant professor for Inorganic Photoactive Materials at the Heinrich-Heine University Düsseldorf, Germany. His group works on the development of inorganic phosphors for e.g., thermometry, LEDs, or upconversion.

2. Experimental section

2.1. Synthesis

Microcrystalline powder of SrB_4O_7:0.5% Sm^{2+} was prepared by a conventional solid-state method as reported earlier.[35] In detail, $SrCO_3$ (Aldrich, ≥99.9%), H_3BO_3 (ChemSolute, ≥99.5%), and the appropriate fraction of Sm_2O_3 (abcr Chemicals, 99.999%) were intimately mixed in an agate mortar and pre-heated at 550 °C for 5 h with a ramp of 150 °C h^{-1} in a corundum crucible. After natural cooling to room temperature, the sintered powder was again intimately ground for 10 min and finally treated at 850 °C with the same heating ramp overnight. This heating step was repeated two more times with intermediate grinding steps. A reducing atmosphere was generated by placing the corundum crucibles on a bed of active charcoal in the

heating steps at 850 °C. The obtained powder was colourless and showed slight red luminescence upon excitation with a 365 nm UV lamp (10 W).

2.2. Characterization and methods

The purity of all microcrystalline samples was verified by powder X-ray diffraction in Debye-Scherrer/transmission geometry (Stoe & Cie STADI P, Cu $K_{\alpha 1}$ radiation filtered by a focussing Ge(111) monochromator, λ = 1.5406 Å; see Fig. S1 in the ESI†).

Optical measurements were performed on an FLS1000 photoluminescence spectrometer from Edinburgh Instruments equipped with a 450 W Xe arc lamp as an excitation source, double excitation and emission monochromators in Czerny-Turner configuration and a thermoelectrically cooled (−20 °C) photomultiplier tube PMT-980. The emission spectra were corrected with respect to the grating efficiency and PMT sensitivity, while excitation spectra were additionally corrected with respect to the lamp intensity. The decay traces of the intense $^5D_0 \rightarrow {}^7F_0$-based emission of Sm^{2+} were measured with a laser diode VPL-420 (Edinburgh Instruments, 70 mW average incident peak power, λ = 423.2 nm) with adjustable temporal pulse width (0.1 μs…1 ms) and variable trigger frequency (0.1 Hz…5 MHz) as the pulsed excitation source. The laser could also be used in a continuous wave excitation mode. The detection mode for the time-resolved measurements was single-photon multi-channel scaling.

Temperature-dependent measurements were performed with a Linkam Scientific THMS600 temperature cell with temperature accuracy of ± 0.1 °C in the regarded temperature range between room temperature and 300 °C. The temperature intervals were 25 °C.

3. Results and discussion

3.1. High-resolution luminescence spectra of Sm^{2+} in SrB_4O_7

Fig. 1 depicts high-resolution photoluminescence excitation and emission spectra of SrB_4O_7:0.5% Sm^{2+} at room temperature. While the excitation spectra are dominated by broad bands due to electric dipole allowed interconfigurational $4f^6 \rightarrow 4f^5 5d^1$ transitions, the emission spectra at room temperature are dominated by the very narrow line emission due to the intraconfigurational $4f^6(^5D_0) \rightarrow 4f^6(^7F_J)$ transitions.[36,37] The most intense line at 685 nm stems from the actually strongly forbidden $^5D_0 \rightarrow {}^7F_0$ transition. The strong intensity is in stark contrast to most known cases of Eu^{3+}-activated phosphors, in which that transition is only very weak (a known exception is, however, LaOBr:Eu^{3+}[38]). This transition has also been considered a potential alternative for optical pressure sensing of the narrow R emission lines of Cr^{3+} in ruby (Al_2O_3:Cr^{3+}).[36,39]

The high intensity of the $^5D_0 \rightarrow {}^7F_0$ transition of Sm^{2+} is not readily explicable within the framework of Judd-Ofelt intensity theory of the $4f^n$-$4f^n$ transitions but can be well-understood with the Wybourne-Downer mechanism instead.[40–43] It is attributed to the high intensity of the induced electric dipole character to the $^5D_0 \rightarrow {}^7F_0$ transition mediated by a spin–orbit interaction between the $4f^6$ and $4f^5 5d^1$ levels of Sm^{2+}, which is a third-order perturbative effect only. Since the $4f^5 5d^1$ configuration is, however, energetically much closer to the $^5D_0$ level in the case of Sm^{2+} in most inorganic host compounds, the Wybourne-Downer mechanism has a significant contribution. The strong $^5D_0 \rightarrow {}^7F_0$-related line is accompanied by small peaks with an average separation of 90 cm^{-1} that can be assigned to vibronic sidebands.[31] Their presence, together with the very narrow linewidth of the $4f^6$–$4f^6$ transitions of Sm^{2+} indicates very weak vibronic coupling of the $4f^6$ levels, which is a characteristic feature of all $4f^n$–$4f^n$ emissions of divalent and trivalent middle lanthanoid ions.[44,45]

A closer inspection of the luminescence spectra also reveals the presence of weak emission peaks from the higher energetic $^5D_1$ spin–orbit level of Sm^{2+} in the range between 620 nm and

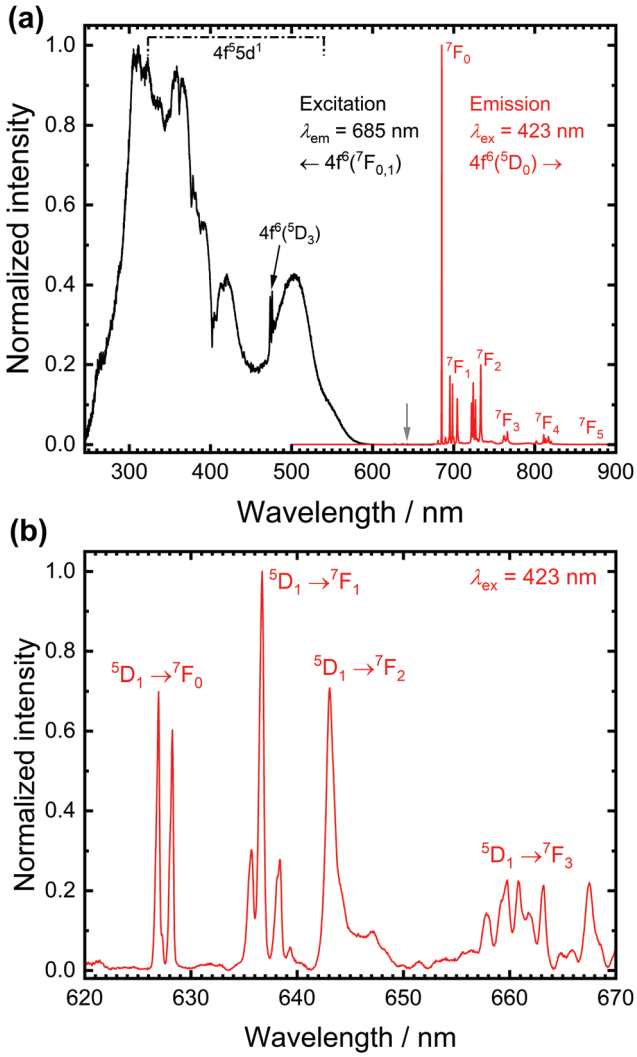

Fig. 1 (a) Photoluminescence excitation (black, λ_{em} = 685 nm) and emission (red, λ_{ex} = 423 nm) spectrum of SrB_4O_7:0.5% Sm^{2+} at room temperature. The emission lines are assigned to the $^5D_0 \rightarrow {}^7F_J$ (J = 0…6) transitions of Sm^{2+}. (b) High-resolution spectrum in the spectral range marked with the grey arrow in (a) indicates the presence of weak $^5D_1 \rightarrow {}^7F_J$ transitions.

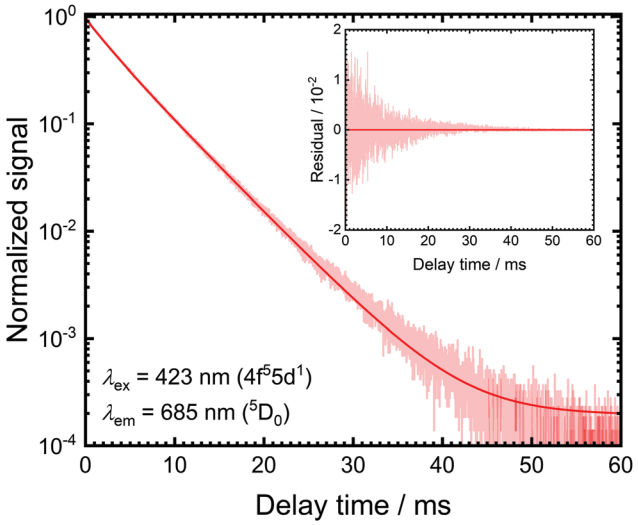

Fig. 2 The photoluminescence decay curve recorded upon monitoring the $^5D_0 \rightarrow {}^7F_0$ transition at 685 nm (λ_{ex} = 423 nm) at room temperature. The solid red line indicates a single exponential fit and the inset depicts the respective residual plot.

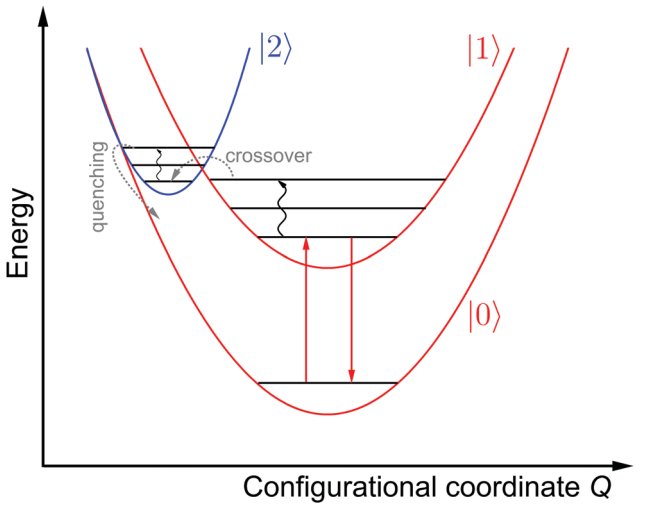

Fig. 3 Schematic overview of the different processes determining the performance of a luminescent crossover thermometer such as Sm^{2+}. Curvy arrows indicate (multi-)phonon absorption transitions. Note that the excited state |2⟩ has been depicted at lower configurational coordinates to match the theoretical and experimental findings for low excited $4f^{n-1}5d^1$ states of lanthanoid ions (see also text).

650 nm (see Fig. 1(b)). The luminescence spectra allow the determination of a $^5D_1$–$^5D_0$ separation of ΔE_{10} = 1330 cm^{-1}, in excellent agreement with literature-reported values.[31,32,46] The presence of the three resolved lines for the $^5D_1 \rightarrow {}^7F_0$ and $^5D_0 \rightarrow {}^7F_1$ transition, respectively, is compatible with the local C_S symmetry at the Sr sites in SrB_4O_7.

The luminescence decay traces upon excitation with 423 nm and monitoring the emission from the $^5D_1$ and $^5D_0$ levels are depicted in Fig. 2. Both show purely single exponential decay at room temperature. The energy separation between the $^5D_0$ and lower energetic $^7F_6$ levels is around 10 000 cm^{-1} and the cut-off phonon energy of SrB_4O_7 is around 1300 cm^{-1}. In addition, no $4f^5d^1 \rightarrow 4f^6$ broad-band luminescence is detectable at room temperature. Thus, decay from the $^5D_0$ = |1⟩ level can be assumed to be purely radiative at 298 K with a radiative decay rate of k_{1r} = (0.193 ± 0.001) ms^{-1}, which agrees perfectly well with previously reported rates.[31,32,46]

3.2. Model for configurational crossover thermometers over a wide temperature range

Fig. 3 schematically depicts the potential energy curves of the excited $^5D_0$ and $4f^5d^1$-related electronic levels of Sm^{2+} projected in configurational coordinate space, which are relevant for a thermal configurational crossover. It has been convincingly shown both theoretically[47–50] and experimentally[35,51–55] that upon excitation into the lowest energetic states of a $4f^n5d^1$ configuration (n = 1, 5, 6, 12, 13), the lanthanoid-ligand distance decreases slightly. However, it should be noted that also a parabola with higher equilibrium distances would not change the following discussion. This is relevant for *e.g.* organic luminophors displaying thermally activated delayed fluorescence (TADF).

Thus, the potential energy curves of the lowest excited $4f^5d^1$ and $4f^6(^5D_0)$ levels will necessarily cross. Moreover, the nature of the chemical metal-ligand bond in both states differs, translating into different curvatures of the potential energy curves. This case has been thoroughly treated theoretically by Struck and Fonger assuming harmonic potentials, which is a reasonable approximation in crystalline solids.[56] They could show that for the two excited levels |2⟩ and |1⟩ with $\Delta E_{21} \geq 10^3$ cm^{-1} and non-negligible configurational coordinate offset, the non-radiative absorption rate can be described by Mott's formula,

$$k_{nr}^{abs}(T) = k_{nr}(0)\exp\left(-\frac{\Delta E_{X1}}{k_B T}\right) \quad (1)$$

with $k_{nr}(0)$ as the intrinsic coupling rate and ΔE_{X1} as the energy gap between the vibrational ground level of the bottom electronic state and the configurational crossover point.

In most typical cases, the activation barrier ΔE_{2X} from the vibrational ground level of the higher excited electronic state to the configurational crossover point is much lower, typically even $\Delta E_{2X} \ll k_B T$. Consequently, the corresponding non-radiative emission rate from the higher excited to the lower excited level is usually dominated by the intrinsic coupling rate $k_{nr}(0)$ and has a weak to negligible temperature dependence.

The steady-state population density ratio of the two excited levels can be generally derived as[13,14]

$$\frac{n_2}{n_1} = \frac{\alpha_{a2}k_{1r} + (\alpha_{a1} + \alpha_{a2})k_{nr}^{abs}(T)}{\alpha_{a1}k_{2r} + (\alpha_{a1} + \alpha_{a2})k_{nr}^{em}(T)} \quad (2)$$

with α_{a1} and α_{a2} as the feeding ratios from a pumped excited auxiliary level |a⟩ to the excited levels |2⟩ and |1⟩ of interest. Using eqn (1) and the previously justified assumption of a temperature-independent non-radiative emission rate,

we obtain

$$R_{21}(T) = \frac{I_2}{I_1} = C\frac{n_2}{n_1} = C\frac{\alpha_{a2}k_{1r} + (\alpha_{a1}+\alpha_{a2})k_{nr}(0)\exp\left(-\frac{\Delta E_{X1}}{k_B T}\right)}{\alpha_{a1}k_{2r} + (\alpha_{a1}+\alpha_{a2})k_{nr}(0)} \quad (3)$$

with C as an electronic pre-factor connecting the luminescence intensity ratio (LIR) with the population ratio. C contains the radiative rates of the excited levels. If the intensities are integrated over all different possible ground levels (to avoid incorporation of emission branching ratios) and upon introduction of $k_{eff} = \alpha_{a1}k_{2r} + (\alpha_{a1}+\alpha_{a2})k_{nr}(0)$, it follows (see ESI† for a detailed derivation),

$$R_{21}(T) = \frac{I_2}{I_1} = \frac{\alpha_{a2}k_{2r}}{k_{eff}} + \frac{k_{2r}}{k_{1r}}\frac{(\alpha_{a1}+\alpha_{a2})k_{nr}(0)}{k_{eff}}\exp\left(-\frac{\Delta E_{X1}}{k_B T}\right) \equiv A + B\exp\left(-\frac{\Delta E_{X1}}{k_B T}\right) \quad (4)$$

Thus, the LIR simply follows an effective or "quasi"-Boltzmann-type law with constant offset at low temperatures, which was also experimentally found earlier already but was lacking theoretical justification so far.[32,57]

The relative sensitivity, $S_r(T)$, is often considered a figure-of-merit for luminescent thermometers. For the case of a configurational crossover thermometer with the LIR obeying eqn (4), S_r is given by

$$S_r(T) = \frac{1}{R_{21}}\left|\frac{dR_{21}}{dT}\right| = \frac{\Delta E_{X1}}{k_B T^2}\left[1 + \frac{A}{B}\exp\left(\frac{\Delta E_{X1}}{k_B T}\right)\right]^{-1} \quad (5)$$

Unlike the relative sensitivity of a conventional Boltzmann thermometer $\left(S_r(T) = \frac{\Delta E_{X1}}{k_B T^2}\right)$, the relative sensitivity of a crossover thermometer goes through a maximum at a specific temperature T_{opt} (in this case $T_{opt} \sim 400$ K) dependent on the relative size of the different radiative and non-radiative rates encoded in the ratio A/B. Only at high temperatures ($k_B T \gtrsim \Delta E_{X1}$) and small ratios of A/B does the relative sensitivity of a crossover thermometer agree with that of a conventional Boltzmann thermometer. It should be noted, however, that it is the interplay between the relative sensitivity and high signal-to-noise ratio that defines the practically actually relevant quantity of statistical precision of a luminescent thermometer.[13,58,59] The statistically expected relative temperature uncertainty is given by

$$\frac{\sigma_T}{T} = \frac{1}{S_r(T)T}\frac{1}{\sqrt{I_1}}\sqrt{1 + \frac{1}{R_{21}(T)}} \quad (6)$$

with $R_{21}(T)$ and $S_r(T)$ as given in eqn (4) and (5), respectively. Formula (6) is valid under the assumption of Poissonian photon counting statistics of the photodetector, which is given for a photomultiplier.

3.2. Case study: configurational crossover thermometry with Sm^{2+} ($4f^6$)

We demonstrate the concept of a configurational crossover thermometer on SrB_4O_7 : 0.5% Sm^{2+}. Fig. 4(a) depicts the temperature-dependent steady-state luminescence spectra (normalized to the intensity of the most intense $^5D_0 \rightarrow {}^7F_0$ transition) of SrB_4O_7 : 0.5% Sm^{2+}. At higher temperatures, a broad band due to the $4f^55d^1 \rightarrow 4f^6$ transition is clearly visible, in good agreement with earlier findings. The evolution of the LIR with temperature is shown in Fig. 4(b) and can be fitted very accurately by the model (4). An energy gap of (3810 ± 90) cm^{-1} between the $^5D_0$ level and crossover point of the $4f^55d^1$-related level is obtained. This appears reasonable as it is assumed that the zero-phonon energy of the broad-banded $4f^55d^1 \rightarrow 4f^6$-related emission ($E_{0\text{-}0} \approx 17\,700$ cm^{-1} according to

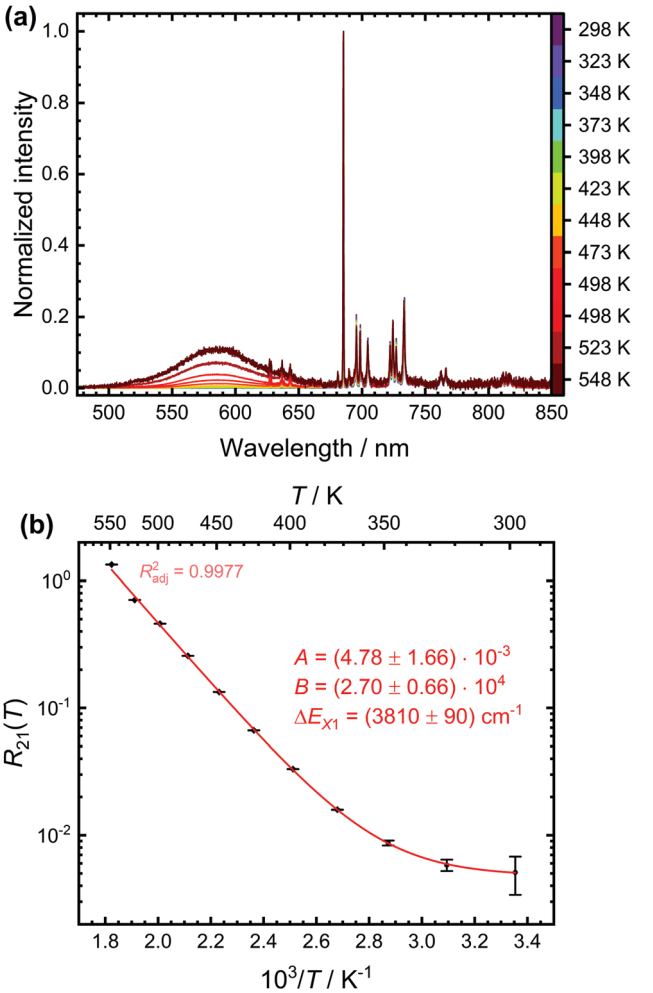

Fig. 4 (a) Temperature-dependent emission spectra of SrB_4O_7 : 0.5% Sm^{2+} (λ_{ex} = 423 nm) normalized to the intensity of the most intense $^5D_0 \rightarrow {}^7F_0$ transition. The peaks on the top of the broad $4f^55d^1 \rightarrow 4f^6$-based emission band stem from the $^5D_1 \rightarrow {}^7F_J$ (J = 0, 1, 2)-related emission. (b) Data (black points) and least-squares fit (red line) according to eqn (4) of the temperature-dependent luminescence intensity ratio between the $4f^55d^1 \rightarrow 4f^6$- and $^5D_0 \rightarrow {}^7F_J$-based emission. The fitting parameters and the adjusted (squared) correlation coefficient indicating the quality of the fit is given as well.

the crossing point between emission and excitation spectrum) should be at the slightly lower energies than the actual crossover point ($E_X \approx 18\,400$ cm^{-1}).

The fitting parameters A and B can also be evaluated in terms of their physical context. According to eqn (4), A basically represents the ratio between the radiative rate of the higher excited level and an effective overall rate containing both the radiative and intrinsic non-radiative crossover transition rate. In a crossover thermometer, it is usually $k_{nr}(0) \gg k_{2r}$, as estimated from the temperature dependence of the $^5D_0$ related decay time (see Fig. S2 in the ESI†) or reported for other Sm^{2+}-activated compounds such as the matlockite-type fluoridochlorides $MFCl$ (M = Ca, Sr, Ba).[60] Thus, A is expectedly to be very small ($A \ll 1$). This is also found from the fit of the temperature-dependent luminescence data in SrB_4O_7 : 0.5% Sm^{2+}, for which $A = (4.78 \pm 1.66) \times 10^{-3}$. The parameter B consists of two factors according to eqn (4). On the one hand, it contains the ratio of the radiative rates of the two excited levels coupled with the crossover process. While $k_{1r} = (0.193 \pm 0.001)$ ms^{-1}, the radiative rate of the $4f^55d^1 \rightarrow 4f^6$-based emission could not be reliably determined with our equipment as it only gains appreciable intensity at higher temperatures and the overall decay is dominated by the non-radiative relaxation rate then. However, it is known for most Sm^{2+}-doped phosphors that the radiative rate of a $4f^55d^1 \rightarrow 4f^6$ transition is in the order of 1–10 μs^{-1}.[61–63] Thus, the order of magnitude of the factor $\frac{k_{2r}}{k_{1r}}$ is expectedly 10^3–10^4. The second factor contained in B relates the intrinsic non-radiative crossover coupling rate $k_{nr}(0)$ to the effective total relaxation rate of the $4f^55d^1$ level also dominated by $k_{nr}(0)$. This factor should be expected to be of the order of 1. Thus, B is overall expected to be in the order of 10^3–10^4. From the least-squares fit of the model (4) to the temperature-dependent LIR, a value of $B = (2.70 \pm 0.66) \cdot 10^4$ is derived, which perfectly agrees with the previous estimates. The presented calibration model for crossover thermometers allows the physical interpretation that can be independently verified by time-resolved measurements and thus, in principle, simulated independently from the experiment.

The expected relative sensitivity and relative temperature uncertainty of the luminescent crossover thermometer SrB_4O_7 : 0.5% Sm^{2+} are depicted in Fig. 5. The relative sensitivity of the tetraborate shows a maximum at around 400 K with a value of 2.98% K^{-1}, similar to earlier reports.[32] Both the temperature and the value of the relative sensitivity depend on the interplay between ΔE_{X1} and the ratio A/B and thus, basically intrinsic electronic properties of the emitting luminescent centre. The practically more relevant quantity of a (relative) temperature measurement uncertainty can be particularly controlled by the emission intensity I_1 of the lower excited level.[13,58,59] Since Sm^{2+} is a very bright emitter in SrB_4O_7 that can be even efficiently excited due to the electric-dipole allowed nature of the $4f^6 \rightarrow 4f^55d^1$ transition, the statistically expected relative temperature uncertainty is typically below 0.1% even for integrated intensities of the $^5D_0 \rightarrow {}^7F_J$-based emission as low as 10^6 counts (see Fig. 5(b)). Due to the efficient thermal coupling

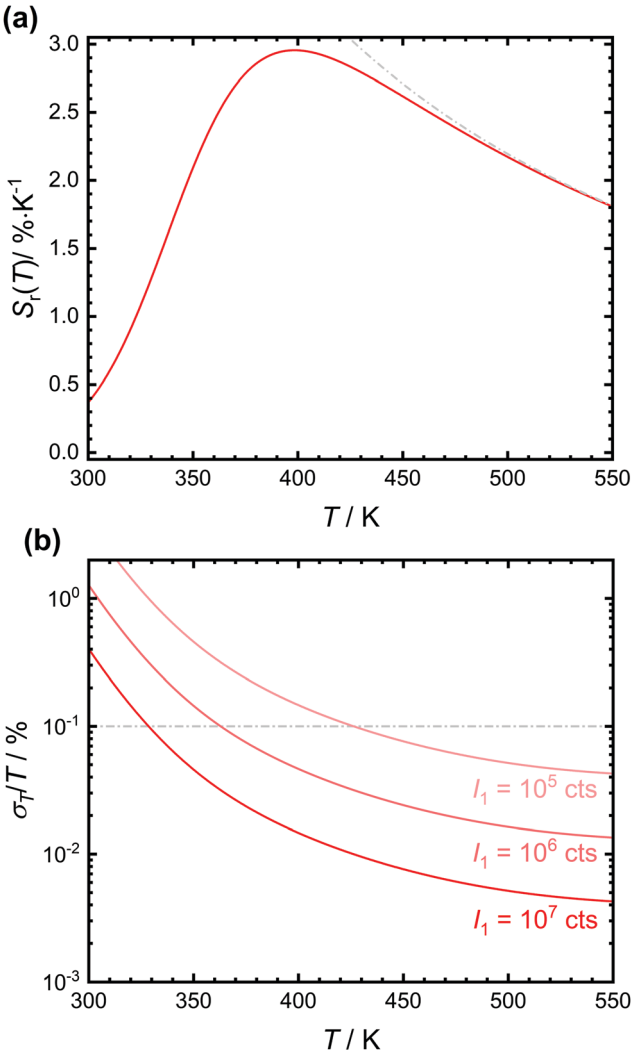

Fig. 5 (a) Plot of the relative sensitivity, $S_r(T)$, of the anticipated luminescent crossover thermometer SrB_4O_7 : 0.5% Sm^{2+} using the fitting values from the plot in Fig. 4(b). The expected relative sensitivity of a purely Boltzmann-based luminescent thermometer with energy gap $\Delta E_{X1} = 3810$ cm^{-1} is also indicated in grey colour. (b) Expected relative statistical temperature uncertainties of SrB_4O_7 : 0.5% Sm^{2+} with different integrated intensities of the $^5D_0 \rightarrow {}^7F_J$ transitions.

between the two excited levels, crossover thermometers are therefore a very promising class of effective luminescent thermometers since high energy gaps can be exploited at rather low temperatures (here > 400 K) in contrast to *e.g.* Boltzmann thermometers. At lower temperatures, the vanishing intensity of the broad $4f^55d^1 \rightarrow 4f^6$ emission band leads to a strong increase in the statistical relative measurement uncertainty above 1%.

It should not be misinterpreted, however, that crossover thermometers can be readily used for wide ranges. Due to the configurational coordinate shift of one of the excited state potentials, not only a crossover to an excited level of interest but also to the ground-level potential is possible. Given the high non-radiative coupling rates $k_{nr}(0)$ between the $4f^55d^1$- and $4f^6$-based levels, thermal quenching of the luminescence is a

serious problem at high temperatures (see also Fig. 3), as was already demonstrated several times for transition metal ions by the Marciniak group[64,65] or in dual-centre luminescent thermometers by *e.g.* Kaczmarek *et al.*[66] Thus, despite the promising relative sensitivities and high measurement precision, crossover thermometers are usually reasonably applicable in a limited temperature range only. This is different from conventional luminescent Boltzmann thermometers based on two excited levels thermally coupled by multiphonon transitions. This type of thermometer does not usually suffer from high-temperature quenching, but the slower thermal coupling processes limit the low-temperature threshold above which thermometry with a Boltzmann-type thermometer would be possible. In that regard, luminescent crossover thermometers offer a practical alternative to classical Boltzmann-type luminescent thermometers.

Conclusions

In this work, we discussed the class of ratiometric luminescent crossover thermometers and derived a physically-interpretable calibration model for them. We showed that the luminescence intensity ratio of such a thermometer generally follows a ''quasi''-Boltzmann-type behaviour with constant offset at low temperatures and how to physically interpret the different fitting parameters. Such verifiability is important for critically judging the quality and physical content of a thermometric calibration model.

The concepts were explicitly demonstrated on experimental data of synthesized microcrystalline $SrB_4O_7:0.5\%\ Sm^{2+}$. Sm^{2+} ($4f^6$) has a low energetic excited $4f^55d^1$ configuration that allows a configurational crossover from the excited $^5D_0$ level of the $4f^6$ configuration. While the luminescence of $SrB_4O_7:0.5\%\ Sm^{2+}$ at room temperature is dominated by narrow line emission due to the $^5D_0 \rightarrow {}^7F_J$ ($J = 0$–6) transitions of Sm^{2+} with a particularly strong $^5D_0 \rightarrow {}^7F_0$-based emission line at 685 nm, a broad-banded $4f^65d^1 \rightarrow 4f^7$-based emission with a maximum at 585 nm emerges at temperatures above 400 K. The temperature-dependent luminescence intensity ratio defined by the integrated intensities of the $4f^65d^1 \rightarrow 4f^7$- and $^5D_0 \rightarrow {}^7F_J$-based emission can be fitted very well with the presented model and the fitting parameters related to the excited state kinetic data. A maximum relative sensitivity of almost $3\%K^{-1}$ at around 400 K was derived. Together with the high luminescence intensity of the $^5D_0 \rightarrow {}^7F_J$ based emission of Sm^{2+} in SrB_4O_7, relative statistical temperature measurement uncertainty below 0.1% can be retained above 400 K. However, despite the promising performance values, crossover thermometers suffer from severe thermal quenching of the luminescence at high temperatures ($T > 548$ K), which poses an upper threshold to the dynamic working range of this type of luminescent thermometers. This is different from classic Boltzmann thermometers, which usually do not suffer from this limitation but are rather insensitive and thus, less precise at high temperatures. Nonetheless, the presented calibration model with the possibility of explicit verification of the physical content offers a way to design luminescent thermometers with desirable performance properties.

Author contributions

B. B. performed the synthesis, characterization, and optical measurements. M. S. supervised the project, analysed the data, and wrote the manuscript. All authors agreed on the final version of the manuscript.

Conflicts of interest

There are no conflicts to declare.

Acknowledgements

The authors would like to thank Prof. Dr W. Frank and Dr G. Kreiner at the Heinrich Heine University for the possibility of and assistance in the usage of the powder X-ray diffraction facilities at their institute.

References

1 C. D.-S. Brites, S. Balabhadra and L. D. Carlos, Lanthanide-Based Thermometers: At the Cutting-Edge of Luminescence Thermometry, *Adv. Opt. Mater.*, 2019, **7**, 1801239.
2 M. D. Dramićanin, Trends in Luminescence Thermometry, *J. Appl. Phys.*, 2020, **128**, 40902.
3 A. Bednarkiewicz, J. Drabik, K. Trejgis, D. Jaque, E. Ximendes and L. Marciniak, Luminescence based temperature bio-imaging: Status, challenges, and perspectives, *Appl. Phys. Rev.*, 2021, **8**, 11317.
4 T. Hartman, R. G. Geitenbeek, G. T. Whiting and B. M. Weckhuysen, Operando monitoring of temperature and active species at the single catalyst particle level, *Nat. Catal.*, 2019, **2**, 986–996.
5 T. P. van Swieten, T. van Omme, D. J. van den Heuvel, S. J.-W. Vonk, R. G. Spruit, F. Meirer, H. H.-P. Garza, B. M. Weckhuysen, A. Meijerink, F. T. Rabouw and R. G. Geitenbeek, Mapping Elevated Temperatures with a Micrometer Resolution Using the Luminescence of Chemically Stable Upconversion Nanoparticles, *ACS Appl. Nano Mater.*, 2021, **4**, 4208–4215.
6 A. Skripka, D. Méndez González, R. Marin, E. Ximendes, B. del Rosal, D. Jaque Garcia, P. Rodriguez Sevilla, D. Mendez-Gonzalez, D. Jaque and P. Rodríguez-Sevilla, Near infrared bioimaging and biosensing with semiconductor and rare-earth nanoparticles: recent developments in multifunctional nanomaterials, *Nanoscale Adv.*, 2021, **3**, 6310–6329.
7 C. D.-S. Brites, X. Xie, M. L. Debasu, X. Qin, R. Chen, W. Huang, J. Rocha, X. Liu and L. D. Carlos, Instantaneous ballistic velocity of suspended Brownian nanocrystals measured by upconversion nanothermometry, *Nat. Nanotechnol.*, 2016, **11**, 851–856.

8 A. R.-N. Bastos, C. D.-S. Brites, P. A. Rojas-Gutierrez, C. DeWolf, R. A.-S. Ferreira, J. A. Capobianco and L. D. Carlos, Thermal Properties of Lipid Bilayers Determined Using Upconversion Nanothermometry, *Adv. Funct. Mater.*, 2019, **29**, 1905474.

9 A. R.-N. Bastos, C. D.-S. Brites, P. A. Rojas-Gutierrez, R. A.-S. Ferreira, R. L. Longo, C. DeWolf, J. A. Capobianco and L. D. Carlos, Thermal properties of lipid bilayers derived from the transient heating regime of upconverting nanoparticles, *Nanoscale*, 2020, **12**, 24169–24176.

10 A. Ćirić, Ł. Marciniak and M. D. Dramićanin, Luminescence intensity ratio squared—A new luminescence thermometry method for enhanced sensitivity, *J. Appl. Phys.*, 2022, **131**, 114501.

11 J. Drabik and L. Marciniak, Excited State Absorption for Ratiometric Thermal Imaging, *ACS Appl. Mater. Interfaces*, 2021, **13**, 1261–1269.

12 A. Paściak, A. Pilch-Wróbel, Ł. Marciniak, P. J. Schuck and A. Bednarkiewicz, Standardization of Methodology of Light-to-Heat Conversion Efficiency Determination for Colloidal Nanoheaters, *ACS Appl. Mater. Interfaces*, 2021, **13**, 44556–44567.

13 M. Suta and A. Meijerink, A theoretical framework for ratiometric single ion luminescent thermometers - Thermodynamic and kinetic guidelines for optimized performance, *Adv. Theory Simul.*, 2020, **3**, 2000176.

14 R. G. Geitenbeek, H. W. de Wijn and A. Meijerink, Non-Boltzmann Luminescence in $NaYF_4$:Eu^{3+}: Implications for Luminescence Thermometry, *Phys. Rev. Appl.*, 2018, **10**, 64006.

15 R. Piñol, J. Zeler, C. D.-S. Brites, Y. Gu, P. Téllez, A. N. Carneiro Neto, T. E. da Silva, R. Moreno-Loshuertos, P. Fernandez-Silva, A. I. Gallego, L. Martinez-Lostao, A. Martínez, L. D. Carlos and A. Millán, Real-Time Intracellular Temperature Imaging Using Lanthanide-Bearing Polymeric Micelles, *Nano Lett.*, 2020, **20**, 6466–6472.

16 T. P. van Swieten, D. Yu, T. Yu, S. J.-W. Vonk, M. Suta, Q. Zhang, A. Meijerink and F. T. Rabouw, A Ho^{3+}-Based Luminescent Thermometer for Sensitive Sensing over a Wide Temperature Range, *Adv. Opt. Mater.*, 2021, **9**, 2001518.

17 A. N. Carneiro Neto, E. Mamontova, A. M.-P. Botas, C. D.-S. Brites, R. A.-S. Ferreira, J. Rouquette, Y. Guari, J. Larionova, J. Long and L. D. Carlos, Rationalizing the Thermal Response of Dual-Center Molecular Thermometers: The Example of an Eu/Tb Coordination Complex, *Adv. Opt. Mater.*, 2022, **10**, 2101870.

18 V. Trannoy, A. N. Carneiro Neto, C. D.-S. Brites, L. D. Carlos and H. Serier-Brault, Engineering of Mixed Eu^{3+}/Tb^{3+} Metal–Organic Frameworks Luminescent Thermometers with Tunable Sensitivity, *Adv. Opt. Mater.*, 2021, **9**, 2001938.

19 S. Otto, N. Scholz, T. Behnke, U. Resch-Genger and K. Heinze, Thermo-Chromium: A Contactless Optical Molecular Thermometer, *Chem. – Eur. J.*, 2017, **23**, 12131–12135.

20 M. Back, J. Ueda, M. G. Brik and S. Tanabe, Pushing the Limit of Boltzmann Distribution in Cr^{3+}-Doped CaHfO3 for Cryogenic Thermometry, *ACS Appl. Mater. Interfaces*, 2020, **12**, 38325–38332.

21 M. Back, J. Ueda, H. Nambu, M. Fujita, A. Yamamoto, H. Yoshida, H. Tanaka, M. G. Brik and S. Tanabe, Boltzmann Thermometry in Cr^{3+}-Doped Ga_2O_3 Polymorphs: The Structure Matters!, *Adv. Opt. Mater.*, 2021, **9**, 2100033.

22 C. D.-S. Brites, K. Fiaczyk, J. F.-C. B. Ramalho, M. Sójka, L. D. Carlos and E. Zych, Widening the Temperature Range of Luminescent Thermometers through the Intra- and Inter-configurational Transitions of Pr^{3+}, *Adv. Opt. Mater.*, 2018, **6**, 1701318.

23 M. Sójka, J. F.-C. B. Ramalho, C. D.-S. Brites, K. Fiaczyk, L. D. Carlos and E. Zych, Bandgap Engineering and Excitation Energy Alteration to Manage Luminescence Thermometer Performance. The Case of $Sr_2(Ge,Si)O_4$:Pr^{3+}, *Adv. Opt. Mater.*, 2019, **7**, 1901102.

24 M. Sójka, C. D.-S. Brites, L. A.-D. Carlos and E. Zych, Exploiting Bandgap Engineering to Fine Control Dual-mode $Lu_2(Ge,Si)O_5$:Pr^{3+} Luminescent Thermometers, *J. Mater. Chem. C*, 2020, **8**, 10086–10097.

25 J. C. Fister, D. Rank and J. M. Harris, Delayed Fluorescence Optical Thermometry, *Anal. Chem.*, 1995, **67**, 4269–4275.

26 C. Baleizão, S. Nagl, S. M. Borisov, M. Schäferling, O. S. Wolfbeis and M. N. Berberan-Santos, An optical thermometer based on the delayed fluorescence of C_{70}, *Chem. – Eur. J.*, 2007, **13**, 3643–3651.

27 H. Uoyama, K. Goushi, K. Shizu, H. Nomura and C. Adachi, Highly efficient organic light-emitting diodes from delayed fluorescence, *Nature*, 2012, **492**, 234–238.

28 A. Steinegger, I. Klimant and S. M. Borisov, Purely Organic Dyes with Thermally Activated Delayed Fluorescence–A Versatile Class of Indicators for Optical Temperature Sensing, *Adv. Opt. Mater.*, 2017, **5**, 1700372.

29 M. Y. Wong and E. Zysman-Colman, Purely Organic Thermally Activated Delayed Fluorescence Materials for Organic Light-Emitting Diodes, *Adv. Mater.*, 2017, **29**, 1605444.

30 A. Steinegger and S. M. Borisov, Zn(II) Schiff Bases: Bright TADF Emitters for Self-referenced Decay Time-Based Optical Temperature Sensing, *ACS Omega*, 2020, **5**, 7729–7737.

31 S. Sakirzanovas, A. Katelnikovas, D. Dutczak, A. Kareiva and T. Jüstel, Concentration influence on temperature-dependent luminescence properties of samarium substituted strontium tetraborate, *J. Lumin.*, 2012, **132**, 141–146.

32 Z. Cao, X. Wei, L. Zhao, Y. Chen and M. Yin, Investigation of SrB_4O_7:Sm^{2+} as a Multimode Temperature Sensor with High Sensitivity, *ACS Appl. Mater. Interfaces*, 2016, **8**, 34546–34551.

33 L. van Pieterson, M. F. Reid, R. T. Wegh, S. Soverna and A. Meijerink, $4f^n \rightarrow 4f^{n-1}5d$ transitions of the light lanthanides: Experiment and theory, *Phys. Rev. B: Condens. Matter Mater. Phys.*, 2002, **65**, 45113.

34 L. R. Morss, Thermochemical properties of Yttrium, Lanthanum, and the Lanthanide Elements and Ions, *Chem. Rev.*, 1976, **76**, 827–841.

35 A. Meijerink, J. Nuyten and G. Blasse, Luminescence and energy migration in $(Sr,Eu)B_4O_7$, a system with a $4f^7$-$4f^6$5d crossover in the excited state, *J. Lumin.*, 1989, **44**, 19–31.

36 A. Lacam and C. Château, High-pressure measurements at moderate temperatures in a diamond anvil cell with a new optical sensor: SrB_4O_7:Sm^{2+}, *J. Appl. Phys.*, 1989, **66**, 366–372.

37 M. Suta and C. Wickleder, Synthesis, spectroscopic properties and applications of divalent lanthanides apart from Eu^{2+}, *J. Lumin.*, 2019, **210**, 210–238.

38 J. Hölsä and P. Porcher, Crystal field effects in REOBr:Eu^{3+}, *J. Chem. Phys.*, 1982, **76**, 2790–2797.

39 T. Zheng, M. Sójka, M. Runowski, P. Woźny, S. Lis and E. Zych, Tm^{2+} Activated SrB_4O_7 Bifunctional Sensor of Temperature and Pressure—Highly Sensitive, Multi-Parameter Luminescence Thermometry and Manometry, *Adv. Opt. Mater.*, 2021, **9**, 2101507.

40 G. W. Burdick, M. C. Downer and D. K. Sardar, A new contribution to spin–forbidden rare earth optical transition intensities: Analysis of all trivalent lanthanides, *J. Chem. Phys.*, 1989, **91**, 1511–1520.

41 M. Tanaka and T. Kushida, Interference between Judd-Ofelt and Wybourne-Downer mechanisms in the $^5D_0$–^7F_J (J = 2,4) transitions of Sm^{2+} in solids, *Phys. Rev. B: Condens. Matter Mater. Phys.*, 1996, **53**, 588–593.

42 M. Tanaka and T. Kushida, Optical transition mechanisms of Sm^{2+} and Eu^{3+} in solids, *J. Lumin.*, 1997, **72-74**, 141–143.

43 O. L. Malta, W. M. Azevedo, E. A. Gouveia and G. F. de Sá, On the $^5D_0 \rightarrow {}^7F_0$ transition of the Eu^{3+} ion in the $\{(C_4H_9)_4N\}_3Y(NCS)_6$ host, *J. Lumin.*, 1982, **26**, 337–343.

44 K.-H. Hellwege, Über die Fluoreszenz und die Kopplung zwischen Elektronentermen und Kristallgitter bei den wasserhaltigen Salzen der Seltenen Erden, *Ann. Phys.*, 1941, **432**, 529–542.

45 A. Ellens, H. Andres, M. L.-H. ter Heerdt, R. T. Wegh, A. Meijerink and G. Blasse, Spectral-line-broadening study of the trivalent lanthanide-ion series. II. The variation of the electron-phonon coupling strength through the series, *Phys. Rev. B: Condens. Matter Mater. Phys.*, 1997, **55**, 180–186.

46 P. Solarz, M. Karbowiak, M. Głowacki, M. Berkowski, R. Diduszko and W. Ryba-Romanowski, Optical spectra and crystal field calculation for SrB_4O_7:Sm^{2+}, *J. Alloys Compd.*, 2016, **661**, 419–427.

47 Z. Barandiarán and L. Seijo, Quantum chemical analysis of the bond lengths in fn and $f^{n-1}d^1$ states of Ce^{3+}, Pr^{3+}, Pa^{4+}, and U^{4+} defects in chloride hosts, *J. Chem. Phys.*, 2003, **119**, 3785–3790.

48 J. L. Pascual, Z. Barandiarán and L. Seijo, Relation between high-pressure spectroscopy and $f^{n-1}d^1$ excited-state geometry: A comparison between theoretical and experimental results in SrF_2:Sm^{2+}, *Phys. Rev. B: Condens. Matter Mater. Phys.*, 2007, **76**, 104109.

49 M. de Jong, A. Meijerink, L. Seijo and Z. Barandiarán, Energy Level Structure and Multiple $4f^{12}5d^1$ Emission Bands for Tm^{2+} in Halide Perovskites: Theory and Experiment, *J. Phys. Chem. C*, 2017, **121**, 10095–10101.

50 J. J. Joos, P. F. Smet, L. Seijo and Z. Barandiarán, Insights into the complexity of the excited states of Eu-doped luminescent materials, *Inorg. Chem. Front.*, 2020, **7**, 871–888.

51 R. Valiente, F. Rodríguez, J. González, H. U. Güdel, R. Martín-Rodríguez, L. Nataf, M. N. Sanz-Ortiz and K. Krämer, High pressure optical spectroscopy of Ce^{3+}-doped $Cs_2NaLuCl_6$, *Chem. Phys. Lett.*, 2009, **481**, 149–151.

52 S. Mahlik, K. Wiśniewski, M. Grinberg and R. S. Meltzer, Temperature and pressure dependence of the luminescence of Eu^{2+}-doped fluoride crystals $Ba_xSr_{1-x}F_2$ (x = 0, 0.3, 0.5 and 1): experiment and model, *J. Phys.: Condens. Matter*, 2009, **21**, 245601.

53 S. Mahlik, M. Grinberg, L. Shi and H. J. Seo, Pressure evolution of $LiBaF_3$:Eu^{2+} luminescence, *J. Phys.: Condens. Matter*, 2009, **21**, 235603.

54 S. Mahlik, A. Lazarowska, M. Grinberg, J.-P. R. Wells and M. F. Reid, Pressure dependence of the emission in CaF_2:Yb^{2+}, *J. Phys.: Condens. Matter*, 2015, **27**, 305501.

55 M. de Jong, D. Biner, K. W. Krämer, Z. Barandiarán, L. Seijo and A. Meijerink, New Insights in $4f^{12}5d^1$ Excited States of Tm^{2+} through Excited State Excitation Spectroscopy, *J. Phys. Chem. Lett.*, 2016, **7**, 2730–2734.

56 C. W. Struck and W. H. Fonger, Unified model of the temperature quenching of narrow-line and broad-band emissions, *J. Lumin.*, 1975, **10**, 1–30.

57 A. Ćirić, S. Stojadinović, Z. Ristić, I. Zeković, S. Kuzman, Ž. Antić and M. D. Dramićanin, Supersensitive Sm^{2+}-Activated Al_2O_3 Thermometric Coatings for High-Resolution Multiple Temperature Read-Outs from Luminescence, *Adv. Mater. Technol.*, 2021, **6**, 2001201.

58 C. Abram, I. Wilson Panjikkaran, S. N. Ogugua and B. Fond, $ScVO_4$:Bi^{3+} thermographic phosphor particles for fluid temperature imaging with sub-°C precision, *Opt. Lett.*, 2020, **45**, 3893–3896.

59 T. P. van Swieten, A. Meijerink and F. T. Rabouw, Impact of Noise and Background on Measurement Uncertainties in Luminescence Thermometry, *ACS Photonics*, 2022, **9**, 1366–1374.

60 Y. Shen and K. L. Bray, Effect of pressure and temperature on 4*f*–4*f* luminescence properties of Sm^{2+} ions in MFCl crystals (M = Ba, Sr, and Ca), *Phys. Rev. B: Condens. Matter Mater. Phys.*, 1998, **58**, 11944–11958.

61 L. C. Dixie, A. Edgar and M. F. Reid, Sm^{2+} fluorescence and absorption in cubic $BaCl_2$: Strong thermal crossover of fluorescence between $4f^6$ and $4f^55d^1$ configurations, *J. Lumin.*, 2012, **132**, 2775–2782.

62 M. Karbowiak, P. Solarz, R. Lisiecki and W. Ryba-Romanowski, Optical spectra and excited state relaxation dynamics of Sm^{2+} ions in $SrCl_2$, $SrBr_2$ and SrI_2 crystals, *J. Lumin.*, 2018, **195**, 159–165.

63 M. Karbowiak and C. Rudowicz, Trends in Hamiltonian parameters determined by systematic analysis of f-d absorption spectra of divalent lanthanides in alkali-halides hosts: II. $CaCl_2$:Ln^{2+} (Ln = Sm, Eu, Tm, and Yb), *J. Lumin.*, 2018, **197**, 66–75.

64 K. Kniec, W. Piotrowski, K. Ledwa, L. D. Carlos and L. Marciniak, Spectral and thermometric properties altering through crystal field strength modification and host material composition in luminescence thermometers based on

Fe^{3+} doped AB_2O_4 type nanocrystals (A = Mg, Ca; B = Al, Ga), *J. Mater. Chem. C*, 2021, **9**, 517–527.

65 K. Kniec, W. Piotrowski, K. Ledwa, M. Suta, L. D. Carlos and L. Marciniak, From quencher to potent activator – Multimodal luminescence thermometry with Fe^{3+} in the oxides MAl_4O_7 (M = Ca, Sr, Ba), *J. Mater. Chem. C*, 2021, **9**, 6268–6276.

66 A. M. Kaczmarek, H. S. Jena, C. Krishnaraj, H. Rijckaert, S. K. P. Veerapandian, A. Meijerink and P. Van der Voort, Luminescent ratiometric thermometers based on a 4f–3d grafted covalent organic framework to locally measure temperature gradients during catalytic reactions, *Angew. Chem., Int. Ed.*, 2021, **60**(7), 3727–3736.